Journal of Alloys and Compounds 509 (2011) 2903–2908

Contents lists available at ScienceDirect

Journal of Alloys and Compounds

journal homepage: www.elsevier.com/locate/jallcom

Non-equilibrium transformation kinetics and primary grain size distribution in the rapid solidification of Fe–B hypereutectic alloy

W. Yang[a,b], F. Liu[a,*], H.F. Wang[a], B.P. Lu[b], G.C. Yang[a]

[a] State Key Laboratory of Solidification Processing, Northwestern Polytechnical University, Xi'an, Shaanxi 710072, PR China
[b] National Defence Key Discipline Laboratory of Light Alloy Processing Science and Technology, Nanchang Hangkong University, Nanchang 330063, PR China

ARTICLE INFO

Article history:
Received 21 October 2010
Received in revised form
20 November 2010
Accepted 23 November 2010
Available online 1 December 2010

Keywords:
Metals and alloys
Rapid-solidification
Phase transitions
Microstructure

ABSTRACT

Considering nucleation, growth and impingement, a numerical model was proposed to describe the transformation kinetics of rapid solidification in bulk undercooled Fe–B hypereutectic alloy. Applying heat balance and solute conservation, the changes of temperature and composition of residual liquid are proved to be not only dependent of time, but also associated with the solidified fraction during the transformation. Accordingly, the driving force for non-equilibrium solidification, as well as the determined nucleation and growth rates, decreases with the process of transformation. On this basis, the primary grain size distribution formed in this process can be predicted with the combination of classical Kolmogorov–Johnson–Mehl–Avrami (KJMA) equation and a probability statistic analysis. Good agreement between the model prediction and experimental results has shown the validity of the proposed model.

1. Introduction

Solidification, the transformation of liquid to solid, occurs as the first step in the fabrication of many metallic materials and plays a fundamental role in the development of microstructure and mechanical properties of final products [1,2]. With non-equilibrium effect, it is possible to produce supersaturated solid solution, amorphous, quasicrystal or nano-crystalline structure, which is unobtainable by using equilibrium solidification methods [3,4]. So, it is important to know the relations between the processing condition and specific transformation information so as to produce the microstructure giving desired properties.

Generally speaking, the non-equilibrium solidification of alloy melts can be performed by rapid quenching [5] and bulk undercooling techniques [6]. The former is realized by enhancing the cooling rate (Φ) and the latter by increasing the initial melt undercooling (ΔT) prior to solidification. Compared with the solidification by rapid heat transfer from melt to environment, the undercooling approach, obtained thermodynamically by suppressing the onset of nucleation upon natural cooling, is advantageous for in situ agnostics, so as to understand the physical mechanism of such rapid transformation.

During the past decades, a great deal of achievements have been made in the field of rapid solidification of undercooled liquid, such as the pioneering work on nucleation performed by Turnbull and coworkers [7,8] and Perepezko and coworkers [9,10], the dendrite growth model developed by Kurz and coworkers [11–13] and the prediction of glass forming ability by Johnson and coworkers [14,15]. However, the theoretical description of primary crystallization kinetics and microstructure formation in undercooled liquid has not been developed to a satisfactory level in comparison with the progresses made for crystallization of amorphous alloys [16–18].

Actually, both the solidification of undercooled liquid and the crystallization of amorphous alloys belong to first-order phase transformation, which consists of nucleation, growth and impingement [19]. However, the amount of latent heat released in amorphous crystallization is so slight that its influence on subsequent transformation can be ignored, which gives the rational basis for the treatment of isothermal or isochronal crystallization. As for solidification of deeply undercooled melts, the prompt release of latent heat from transformed solid increases drastically the melt temperature. In such a case, a new freedom is introduced, so the whole transformation kinetics is not only associated with the elapsed time, but also dependent on the transformed solid fraction.

In dealing with the rapid solidification of bulk undercooled melts, it is generally accepted that two regimes occur, i.e., rapid solidification accompanying recalescence and the subsequent near-equilibrium solidification controlled solely by external heat extraction to the environment. Thermodynamically, the main factor that governs the transformation far from equilibrium is the driving force for nucleation and growth, which decreases

* Corresponding author. Tel.: +86 29 88460374; fax: +86 29 88491000.
E-mail address: liufeng@nwpu.edu.cn (F. Liu).

0925-8388/$ – see front matter © 2010 Elsevier B.V. All rights reserved.
doi:10.1016/j.jallcom.2010.11.152

as transformation proceeds until the establishment of a new equilibrium state between the as-formed solid and residual liquid. With reference to our previous work [20–22], the decreases of nucleation and growth rates of primary phase are associated with the variation of composition and temperature of residual liquid. Applying the proposed model to solid solution and hypereutectic alloys, excellent agreement is achieved between the predicted maximum recalescence temperature and experimental results.

In the present work, quantitative calculations of nucleation and growth rates are performed. On this basis, the previous model [22] was further developed to describe the primary transformation kinetics of bulk undercooled liquid, where the significant effect of released solidification latent on subsequent transformation is considered properly. Moreover, the grain size distribution in the primary solidification, subjected to the effects of nucleation and growth, is presented.

2. Mathematical modeling

As indicated earlier, phase transformation occurs by means of nucleation and growth. Hence, the total transformation kinetics is determined by the nucleation frequency and the growth rate, which are both dependent of the driving force between the residual liquid and the as-formed solid.

2.1. Kinetic transformation model

2.1.1. Nucleation

As the initial domain of solidification, nucleation controls to a large extent the initial structure, the size scale and the spatial distribution of the product phase. On the basis of classical nucleation theory, the atomic thermal fluctuation within a liquid leads to the accidental formation of solid-like clusters (embryos). In such a case, interface develops between the old and the new phases, whereas the production of new phase releases the chemical Gibbs energy and the creation of the interface costs Gibbs energy. The steady-state homogeneous nucleation frequency can be expressed as [7,8]:

$$I_{hom} = \frac{N_V kT}{3\pi a_0^3 \eta} \exp\left(-\frac{\Delta G^*}{kT}\right) \tag{1}$$

where a_0 is the typical interatomic spacing, k the Boltzmann constant, N_V the number of atoms per unit volume, η the viscosity of undercooled liquid, and ΔG^* the activation energy barrier for nucleation, which can be expressed as:

$$\Delta G^* = \frac{16\pi\sigma^3}{3\Delta G_V^2} \tag{2}$$

where $\Delta G_V = \Delta G_m / V_m$ is the change of Gibbs free energy per unit volume with V_m as the molar volume, σ the temperature-dependent solid/liquid interface energy, which can be expressed by using the "diffuse interface" approach [23]:

$$\sigma(T) = \left[0.48 + 0.52\left(\frac{T}{T_m}\right)\right]\sigma(T_m) \tag{3}$$

where $\sigma(T_m)$ is the interfacial energy at the melting point. To estimate this value, the negentropic model proposed by Spaepen [24] is widely used:

$$\sigma = \gamma \frac{\Delta S_f}{N_A^{1/3} V_m^{2/3}} T \tag{4}$$

where γ is the structure factor of solid nucleus and ΔS_f the entropy of fusion.

In practice, alloy melts usually contain impurities, substrates and short-range-order (SRO) structures (such as icosahedral cluster), which may act as the heterogeneous nucleation sites. Accordingly, the heterogeneous nucleation rate can be given as [7,8]:

$$I_{het} = \frac{N_1 kT}{3\pi a_0^3 \eta} \exp\left[-\frac{\Delta G^*}{kT} f(\theta)\right] \tag{5}$$

where N_1 represents the fraction of atoms acting as origin for heterogeneous nucleus. $f(\theta)$ is the catalytic potency factor for heterogeneous nucleation, which depends on the wetting angle θ.

2.1.2. Growth

Most of the rapid solidification processes are believed to take place in the continuous growth regime with a diffuse interface. In such a case, the crystal growth rate can be expressed using the Turnbull's approximation [19]:

$$u(T) = \frac{fD}{a_0}\left[1 - \exp\left(-\frac{\Delta G}{RT}\right)\right] \tag{6}$$

in which f is the fraction of sites at the interface where atoms may preferentially be added or removed, and equals $0.2(T_m - T)/T_m$ for complex structure with T_m as the liquidus temperature. D is the diffusion coefficient, which is related to liquid viscosity η by the Stokes–Einstein expression:

$$D = \frac{kT}{3\pi a_0 \eta} \tag{7}$$

The viscosity η of metallic liquid is approximately expressed by the Vogel–Fulscher–Tammann equation [19]:

$$\eta = A \exp\left(\frac{B}{T - C}\right) \tag{8}$$

where A, B and C are constants typically determined by experimental measurement.

2.1.3. Impingement

Upon nucleation and growth, the volume fraction transformed at a given time is well described by the classical Kolmogorov–Johnson–Mehl–Avrami theory [25,26], which relates the actual transformed fraction with the extended transformed fraction by the following expression:

$$f = 1 - \exp(-f_{ext}) \tag{9}$$

where f_{ext} is the extended transformation fraction that the growing grains would occupy without impingement. Analogous to previous treatment [27], it can be expressed as:

$$f_{ext}(t) = \frac{4\pi}{3}\int_0^t I(T,\tau)[u(T,\tau)]^3 \, d\tau \tag{10}$$

2.1.4. Driving force of transformation

The thermodynamic driving force for nucleation and growth can be obtained by CALPHAD method. For binary system, it can be solved by the following form [28]:

$$\Delta G(c_s, c_l, T) = X_B[\mu_L^B(c_l, T) - \mu_s^B(c_s, T)] + X_A[\mu_L^A(c_l, T) - \mu_s^A(c_s, T)] \tag{11}$$

where μ_L^A and μ_L^B, μ_S^A and μ_S^B are the chemical potentials of component A and B in liquid and solid separately.

Upon solidification, the undercooled melt may itself act as a heat sink to cause a very high solidification rate which in turn increases the residual liquid temperature. For cooling an isothermal melt undergoing a solidification process, the thermal behavior can be described by a simple Newtonian formulation, which considers the

heat capacity, the release of latent heat and the heat transfer to the environment together [29]:

$$\frac{\partial T}{\partial t} = -\frac{Q}{\rho c} + \frac{\Delta H}{\rho c}\frac{\partial f}{\partial t} \tag{12}$$

where ΔH the solidification latent heat, Q (=$\rho c\Phi$) the heat extraction rate due to radiation and convection with ρc as the volume heat capacity.

According to previous studies [27,29], it is reasonable to assume an adiabatic recalescence to minimize the computational requirement, and then Eq. (12) can be rewritten as:

$$\frac{\partial T}{\partial t} = \frac{\Delta H}{\rho c}\frac{\partial f}{\partial t} \tag{13}$$

The above equation can be further expressed in a discrete form [23]:

$$T_{i+1} - T_i = \frac{\Delta H}{\rho c}(f_{i+1} - f_i) \tag{14}$$

where f_i and f_{i+1} are the solidified fraction corresponding to the melt temperature at T_i and T_{i+1}.

With the process of transformation, more and more solute atoms are rejected into residual liquid owing to L/S solute concentration difference. Assuming no back-diffusion in the solid and complete mixing within the residual liquid, the evolution of liquid concentration can be expressed according to the solute conservation principle [22]:

$$c_i = \frac{c_0 - \sum_{j=1}^{i} c_{sj}\Delta f_j}{\left(1 - \sum_{j=1}^{i}\Delta f_j\right)} \tag{15}$$

where c_0 is the initial liquid concentration, Δf_j the calculated solid fraction during the jth step and c_{sj} the corresponding solid concentration.

Particularly for primarily formed intermetallic phase, c_{sj} (holding constant) can be determined directly. Then Eq. (15) can be simplified as:

$$c_l = \frac{c_0 - c_s f}{1 - f} \tag{16}$$

where c_s is the stoichiometry of the as-formed intermetallic phase.

2.2. Distribution of primary grain size

Using the above equations, the time dependence of the volume fraction of new phase can be described well during the transformation. However, the primary grain size, as well as its distribution, is not included, although these microstructure characteristics are also related to the nucleation and growth protocols. In order to solve this problem, the PKJMA mean field statistical model proposed by Crespo et al. [17,18] was herein employed.

Assuming a typical length d, the variable time scale $\tau(t)$ can be determined by the current growth rate, which can be written as:

$$\int_t^{t+\tau(t)} u(T, t')\,dt' = d \tag{17}$$

According to PKJMA model, each grain belonging to the extended populations grows as if it were completely isolated without considering impingement between each other. In such a case, the extended grain size distribution can be written as

$$N^*(1, i+1) = N(\tau_{i+1}) \tag{18}$$

$$N^*(j+1, i+1) = N^*(j, i) \tag{19}$$

where $N^*(j, i)$ is the extended grain number of length j at time i. It should be mentioned that the grain group with length j will completely transform to next group with length $j+1$ after free growth in one time step. $N(\tau_{i+1}) = \int_0^{\tau_{i+1}} I(T, t_{i+1})\,d\tau$ is the newly formed grain during this stage and the total time can be expressed as:

$$t_{i+1} = \sum_{p=1}^{i+1}\tau_p.$$

Because the growth of actual particle may be stopped due to impingement with the neighboring ones, some grains of each population will grow at a reduced rate. Therefore, only a fraction α, but not all, of each population can reach the next volume:

$$N(1, i+1) = N(\tau_{i+1}) + N(1, i)[1 - \alpha(i)] \tag{20}$$

$$N(j+1, i+1) = N(j, i)\alpha(i) + N(j+1, i)[1 - \alpha(i)] \tag{21}$$

where $N(j, i)$ is the actual grain number of length j at time i.

The probability factor α can be achieved by adopting KJMA equation using an iterative method, which relates the actual transformation fraction with the extended transformation fraction from Eq. (9), where the two terms can be given as:

$$f_{ext}^{i+1} = \sum_{j=1}^{i+1}\frac{4\pi}{3}j^3 N^*(j, i+1) \tag{22}$$

$$f^{i+1}(\alpha) = \sum_{j=1}^{i+1}\frac{4\pi}{3}j^3 N(j, i+1) \tag{23}$$

3. Results and discussion

While the mathematical formulation and the solution methodology developed are suitable for both solid solution and intermetallic, a hypereutectic Fe–B alloy is herein used as an example. According to the previous studies and published phase diagram [22,30,31], intermetallic Fe_2B forms primarily during the rapid solidification of this alloy. Note that the defined stoichiometry of this phase gives a more accurate illustration for the above relationships.

Rapid solidification of bulk undercooled $Fe_{78}B_{22}$ alloy melt was performed by melt fluxing method. The experimental apparatus consists of a high frequency induction heating facility, an infrared pyrometer and a signal recorder [21–23]. The heating and cooling curves of the melts were measured by the infrared pyrometer, which was calibrated with a standard PtRh30-/PtRh6 thermocouple, and possesses a relative accuracy of 3 K, and a response time less than 5 ms. At the end of recalescence, samples were rapidly quenched into a Ga–In–Sn bath in order to keep the as-formed microstructure in non-equilibrium solidification. After experiment, the solidified samples were sectioned longitudinally and processed according to standard metallographic procedure. The as-quenched microstructures were examined using scanning electron microscope and the grain size was determined by the linear intercept method. The optimized thermodynamic data for this alloy system [30] was adopted and the basic physical parameters for $Fe_{78}B_{22}$ alloy are given in Table 1 [30,31].

3.1. Non-equilibrium solidification kinetics of $Fe_{78}B_{22}$ alloy

Incorporating Eqs. (1), (5), (6), (9), (14) and (16), the temporal evolution of melt temperature for the samples undercooled by 170 K and 251 K, is shown in Fig. 1. Obviously, the time-temperature profile presents "S" type and the entire time interval for rapid solidification is shortened with increasing undercooling. Moreover, the maximum recalescence temperature reduced from 1225 °C to

Table 1
Physical parameters for the $Fe_{78}B_{22}$ alloy used in the model calculations [30,31].

Parameter		Unit	Value
Heat of solidification	ΔH_f	J/mol	28,035
Specific heat	C_P	J/mol K	50
Gas constant	R_g	J/mol K	8.31451
Equilibrium liquidus temperature	T_m	K	1561
Interatomic spacing	a_0	nm	1.03
Liquid viscosity	η	N/m^2	$3.756 \times 10^{-3} \times \exp(2480/(T-722))$
Catalytic factor	$f(\theta)$	–	0.18
Structure factor	γ	–	0.44

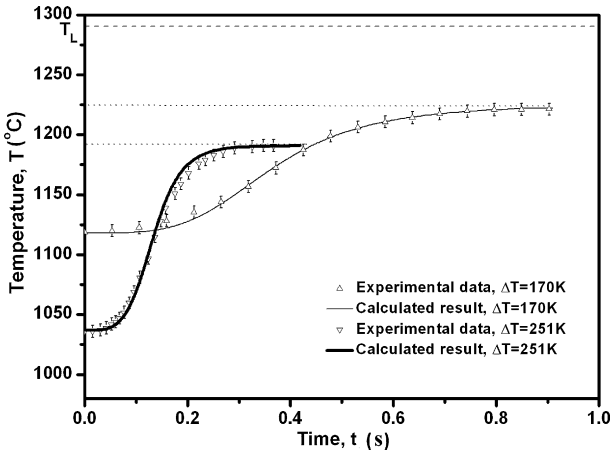

Fig. 1. Variation of liquid temperature as a function of transformation time for $Fe_{78}B_{22}$ alloy undercooled by 170 K and 251 K, respectively.

1194 °C with the increase of initial undercooling. Considering the maximum recalescence temperature and the whole transformation curves, it is evident from these plots that the agreement between theory prediction and experimental measurements is excellent.

To give a better understanding of this transformation, Fig. 2 presents the variation of transformation driving force as a function of undercooling. It can be seen that the driving force is continuously increased with the increase of undercooling. As a consequence, the corresponding nucleation and growth rates for larger driving force are enhanced, which will accelerate the transformation process and shorten the whole transformation time.

Corresponding to Fig. 1, the transformation rate df/dt is presented in Fig. 3, where both curves experience a first increase and then a decrease after reaching its peak maximum, i.e., a typical feature of transformation composed of nucleation and growth. As is predicted, the transformation rate for larger undercooling is faster than that for smaller undercooling.

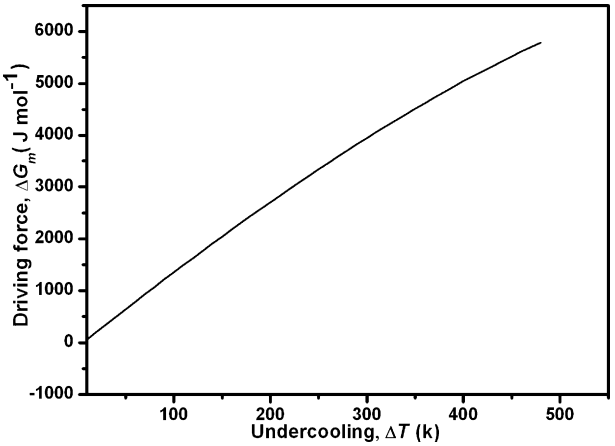

Fig. 2. Variation of liquid/solid transformation driving force as a function of undercooling for $Fe_{78}B_{22}$ alloy.

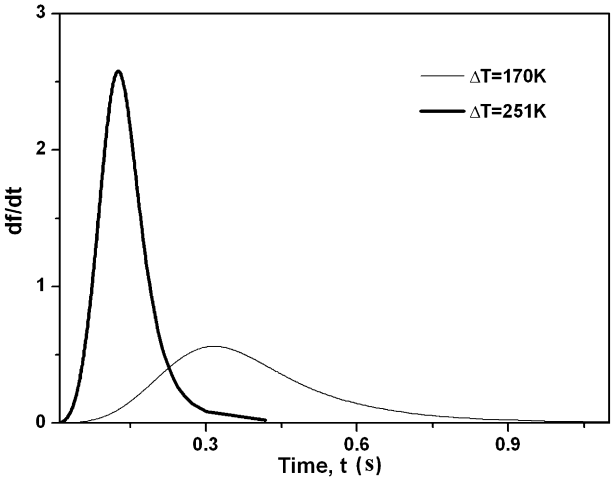

Fig. 3. Variation of solid transformation rate as a function of time during the rapid solidification of $Fe_{78}B_{22}$ alloy at different undercoolings.

In early stage, the growth rate is fast, as can be determined by the larger driving force. However, the actual nucleation number at this time is small, which generates the slower transformation speed. Accompanying the effective increase of grain number, the transformation gradually gathers speed. With the process of transformation, the impingement phenomenon is becoming more severe. Moreover, the melt temperature elevates rapidly. As inferred from the foregoing analysis, it will cause the decrease of the transformation driving force, as well as the nucleation and growth rates. Consequently, the actual transformation speed starts to drop gradually. This point is more clearly illustrated in Fig. 4, which gives the changes of nucleation and growth rate with the increase of melts temperature for sample undercooled by 170 K. One can see that, both the nucleation and growth rates drop with the process of transformation. Compared with the favorable atomic diffusion ability at high temperature, the decrease of driving force is more dominant for this transformation process.

3.2. Grain size distribution in the primarily solidified $Fe_{78}B_{22}$ alloy

As-quenched morphologies of the primarily solidified $Fe_{78}B_{22}$ alloy, subjected to the above two different undercoolings, i.e., $\Delta T = 170$ K and 251 K, are shown in Fig. 5, where the quasi-sphere

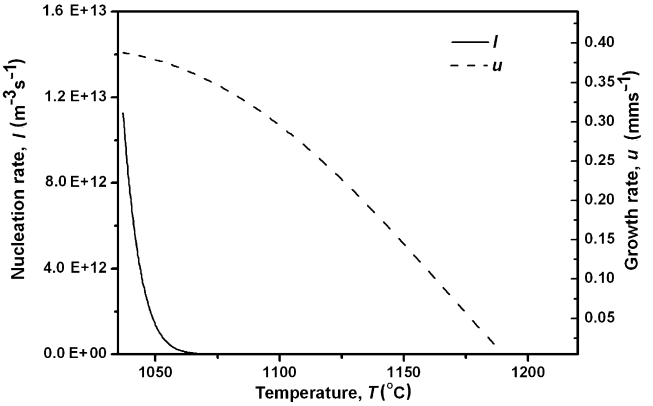

Fig. 4. Nucleation rate and growth rate as functions of temperature during the recalescence of $Fe_{78}B_{22}$ alloy undercooled by 170 K.

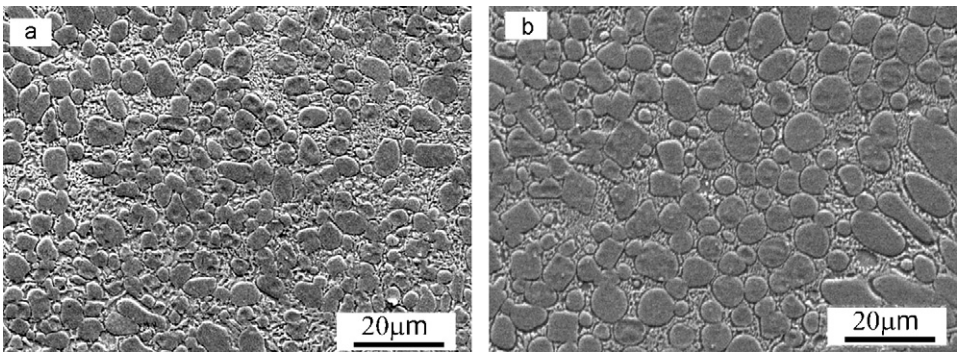

Fig. 5. As-solidified primary microstructures of $Fe_{78}B_{22}$ alloy at different undercoolings: (a) ΔT = 170 K; (b) ΔT = 251 K.

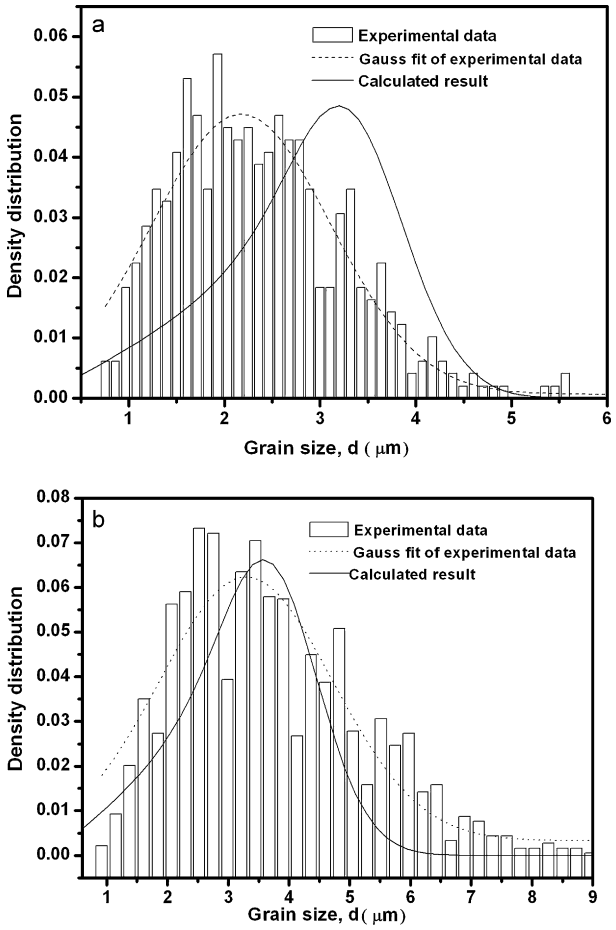

Fig. 6. Experimental and calculated grain size distribution for $Fe_{78}B_{22}$ alloy at different undercoolings: (a) ΔT = 170 K; (b) ΔT = 251 K.

grains distribute randomly in the matrix. As can be seen clearly, both the volume fraction of primary phase and its grain size increases with the enhanced ΔT.

Using Eqs. (20) and (21), the calculated grain size distributions in the primarily solidified morphology, for the samples undercooled by 170 K and 251 K, are illustrated in Fig. 6, separately, where the experimental measurements from Fig. 5 are also compared.[1] Obviously, both curves show a similar Gauss distribution shape and some agreement can be obtained, especially for larger undercooling. With the increase of undercooling, the average grain size is enhanced by a factor of two, which is the result of the aforementioned nucleation and growth processes. As is well known, solidification of a large continuous bulk liquid metal will likely be catalyzed by the heterogeneous nucleation motes inside a melt or the metal oxides at the melt surface and undercooled melts. In melt fluxing experiment, these potential nucleation sites are eliminated through the physical adsorption by molten glass and its chemical reaction with heterogeneities. As a result, less heterogeneous nucleation sites exist for larger undercooling, which makes the decrease of effective nucleation number. Moreover, the as-formed grain grows faster for larger undercooling and the promote release of latent heat inhibits the further nucleation process. The combination of less nucleation sites and larger growth rate leads to the increase of grain size of primary phase. The observed discrepancy for small undercooling, i.e., ΔT = 170 K, can mainly be attributed to smaller transformation fraction in this condition, which generates larger experimental uncertainty for measurement.

4. Conclusions

On the basis of quantitative calculation of nucleation and growth protocols, a numerical model for describing the non-equilibrium solidification kinetics for bulk undercooled Fe–B hypereutectic alloy was established with the combination of the phenomenological macroscopic heat flow balance, mass conservation with the microscopic solidification kinetics. Applying a method of probability statistic analysis, the resultant grain size distribution of primary grain can also be predicted and its evolution process has been well explained. Good agreement between the model prediction and experimental results was obtained, showing the validity of present model. The transformation process experiences a first increase and then decrease after reaching its peak point, showing a typical characteristic of nucleation and growth phase transformation.

Acknowledgements

The authors are grateful to the Free Research Fund of State Key Lab. of Solidification Processing (09-QZ-2008; 24-TZ-2009), the 111 project (B08040), the Natural Science Foundation of China (Grant nos. 50771084; 51071127), National Basic Research Program of China (973Program) 2011CB610403, the HuoYingdong Yong Teacher Fund (111052), the Fundamental Research Fund of Northwestern Polytechnical University (2008JC01). The Open Fund of Aeronautical Science and Technology Key Lab. of Aeronautical Materials Processing in Nanchang Hangkong University and the Project of Education Department of Jiangxi (GJJ08199). W. Yang is greatly acknowledge to the financial support by the fund of the State Key Laboratory of Solidification Processing in NWPU

[1] It should be noted that the three-dimension space distribution from the theory prediction must be transformed into the two-dimension plane distribution so as to be compared with the experimental measurements [17,18].

(SKLSP201118) and Scientific Starting Foundation for Doctorate Research in Nanchang Hangkong University (EA201003234).

References

[1] W. Kurz, D.J. Fisher, Fundamentals of Solidification, fourth ed., Trans. Tech. Publications Ltd., Switzerland, 1998.
[2] J.C. Baker, J.W. Cahn, Solidification, first ed., ASM, Metals Park, OH, 1971.
[3] D.M. Herlach, Mater. Sci. Eng. R 12 (1994) 177–272.
[4] L.A. Jacobson, J. Mckittrick, Mater. Sci. Eng. R 11 (1994) 355–408.
[5] Y. Wu, M.V. Lototsky, J.K. Solberg, S.X. Zhou, J. Alloys Compd. 477 (2009) 262–266.
[6] F. Liu, G.C. Yang, Int. Mater. Rev. 51 (2006) 145–170.
[7] D. Turnbull, J.C. Fisher, J. Chem. Phys. 17 (1949) 71–73.
[8] D. Turnbull, J. Appl. Phys. 21 (1950) 804–810.
[9] J.H. Perepezko, J.S. Smith, J. Non-Cryst. Solids 44 (1981) 65–83.
[10] J.H. Perepezko, Mater. Sci. Eng. 65 (1984) 125–135.
[11] J. Lipton, M.E. Glicksman, W. Kurz, Mater. Sci. Eng. A 65 (1984) 57–63.
[12] W.J. Boettinger, S.R. Coriell, R. Trivedi, in: R. Mehrabian, P.A. Parrish (Eds.), Rapid Solidification Processing: Principles and Technologies IV, Claitor's, Baton Rouge, LA, 1988, p. 13.
[13] J. Lipton, W. Kurz, R. Trivedi, Acta Metall. 35 (1987) 957–964.
[14] S. Mukherjee, J. Schroers, Z. Zhou, W.L. Johnson, W.K. Rhim, Acta Mater. 52 (2004) 3689–3695.
[15] J. Schroers, A. Masuhr, W.L. Johnson, Phys. Rev. B 60 (1999) 11855–11858.
[16] W. Sha, X. Wu, K.G. Keong, Electroless Copper and Nickel-Phosphorus Plating: Processing, Characterisation and Modelling, first ed., Woodhead Publishing Limited, Cambridge, 2010.
[17] D. Crespo, T. Pradell, M.T. Clavaguera-Mora, Phys. Rev. B 55 (1997) 3435–3444.
[18] M.T. Clavaguera-Mora, N. Clavaguera, D. Crespo, Prog. Mater. Sci. 47 (2002) 559–619.
[19] J.W. Christian, The Theory of Transformation in Metals and Alloys, third ed., Pergamon Press, Oxford, 2002.
[20] W. Yang, F. Liu, H.F. Wang, G.C. Yang, J. Alloys Compd. 470 (2009) L13–L16.
[21] W. Yang, F. Liu, H.F. Wang, G.C. Yang, Y.H. Zhou, J. Cryst. Growth 311 (2009) 3225–3230.
[22] W. Yang, F. Liu, H. Liu, Z. Chen, G.C. Yang, Y.H. Zhou, J. Alloys Compd. 491 (2010) 118–122.
[23] L. Granasy, J. Non-Cryst. Solids 162 (1993) 301–303.
[24] F. Spaepen, Acta Metall. 23 (1975) 729–743.
[25] M. Avrami, J. Chem. Phys. 7 (1939) 1103–1112.
[26] M. Avrami, J. Chem. Phys. 9 (1941) 177–184.
[27] A.M. Saleh, R.A. Clemente, Jpn. J. Appl. Phys. 43 (2004) 3624–3628.
[28] N. Saunders, A.P. Miodownik, Calculation of Phase Diagrams—A Comprehensive Guide, first ed., Pergamon Press, Oxford, 1998.
[29] T.J. Piccone, Y. Wu, Y. Shiohara, M.C. Flemings, Metall. Trans. A 18 (1987) 925–932.
[30] L. Battezzati, C. Antonione, M. Baricco, J. Alloys Compd. 247 (1997) 164–171.
[31] C.L. Yang, F. Liu, G.C. Yang, Y.Z. Chen, N. Liu, Y.H. Zhou, J. Alloys Compd. 411 (2007) 101–106.